JGR Atmospheres

RESEARCH ARTICLE
10.1029/2023JD040392

Special Section:
Land-atmosphere coupling: measurement, modelling and analysis

Estimation of Soil Moisture Thresholds for Aggravation of Global Terrestrial Carbon Uptake Losses

Heng Yan[1,2], Zhenghui Xie[1,2], Binghao Jia[1], Peihua Qin[1], Xia Zhang[1], Qiudan Dai[1], Jinbo Xie[1], Longhuan Wang[1], Ruichao Li[1], Yuhang Tian[1,2], and Yanbin You[1,2]

[1]State Key Laboratory of Numerical Modeling for Atmospheric Sciences and Geophysical Fluid Dynamics, Institute of Atmospheric Physics, Chinese Academy of Sciences, Beijing, China, [2]College of Earth and Planetary Sciences, University of Chinese Academy of Sciences, Beijing, China

Key Points:

- Simulations conducted by an earth system model estimated the soil moisture thresholds (SMTs) that aggravate global terrestrial carbon uptake losses
- SM-limited ecoregions have higher SMTs than energy-limited ecoregions
- Land-atmosphere feedback caused by SM deficit is one of the reasons for aggravation of terrestrial carbon uptake losses

Correspondence to:
Z. Xie,
zxie@lasg.iap.ac.cn

Citation:
Yan, H., Xie, Z., Jia, B., Qin, P., Zhang, X., Dai, Q., et al. (2024). Estimation of soil moisture thresholds for aggravation of global terrestrial carbon uptake losses. *Journal of Geophysical Research: Atmospheres*, *129*, e2023JD040392. https://doi.org/10.1029/2023JD040392

Received 14 NOV 2023
Accepted 17 FEB 2024

Author Contributions:
Conceptualization: Heng Yan, Zhenghui Xie, Binghao Jia, Peihua Qin, Qiudan Dai, Jinbo Xie, Longhuan Wang, Ruichao Li, Yuhang Tian, Yanbin You
Methodology: Heng Yan, Zhenghui Xie
Validation: Heng Yan
Visualization: Heng Yan
Writing – original draft: Heng Yan
Writing – review & editing: Binghao Jia, Peihua Qin, Qiudan Dai, Longhuan Wang, Ruichao Li, Yuhang Tian, Yanbin You

Abstract Most ecosystems have resistance to soil moisture (SM) deficit, which is termed drought resistance. Drought resistance can be invalid and global terrestrial carbon uptake losses can be aggravated when SM deficit exceeds a critical threshold. However, soil moisture thresholds (SMTs) that detrimentally impact global terrestrial carbon uptake are still unclear. We performed numerical simulations using the Community Earth System Model, and estimated the SMTs by the back propagation neural network method for the years 2004–2014. The SMTs represent the inflection point for vegetation changes from high to low drought resistance phase, and terrestrial carbon uptake losses from low to high rate. Soil moisture-limited ecoregions have higher SMTs than energy-limited ecoregions, indicating the increased vulnerability and sensitivity of SM-limited ecoregions to SM deficit and more easily aggravated terrestrial carbon uptake losses during drought. SMTs varied in different vegetation types and broadleaf deciduous trees displayed the highest SMTs and C3 arctic grasses have lowest thresholds. Humid and high vegetation coverage rate regions have lower thresholds. The SMTs increase with the increase of clay content and the decrease of sand content. In addition, land-atmosphere feedback caused by SM deficit has a large impact on terrestrial carbon uptake and may be one of the main reasons for the aggravation of vegetation carbon uptake losses. Our results provide a unique perspective for investigating the impact of drought on vegetation.

Plain Language Summary With global warming, severe soil moisture (SM) deficit will become more intense, frequent, and will last longer in many regions. Global terrestrial carbon uptake losses can be aggravated when SM deficit exceeds a critical threshold. However, soil moisture thresholds (SMTs) that detrimentally impact global terrestrial carbon uptake are still unclear. The present study fills this gap. SMTs that aggravate global terrestrial carbon uptake losses are estimated. The SMTs for different climate zones and vegetation types are determined. Estimating SMTs is essential for predicting soil drought risk and preparing for future climate change.

1. Introduction

Terrestrial carbon uptake is often measured as gross primary production (GPP). The uptake is affected by a variety of factors, which include solar radiation, temperature water availability and natural disasters (Breshears et al., 2005; Guo et al., 2010; Piao et al., 2019). Vegetation, which is the main route of carbon uptake, experiences the impacts of soil moisture (SM) dynamics, since water is acquired directly from soil (Green et al., 2019; Liu et al., 2020; Lyons et al., 2021). Extensive studies on the response of vegetation to SM deficit have revealed significant impacts of SM on vegetation only when SM is below a critical threshold (Esmaeilzade et al., 2015; Meir et al., 2015; Meng et al., 2022; Oglesby et al., 2002). Strategies of vegetation to mitigate water loss and maintain optimal water supply under drought stress include stomata closure and osmotic regulation to prevent excessive water loss and disruption of xylem water transport (Dannenberg et al., 2022; Gupta et al., 2020; X. Yang et al., 2021). Once the SM deficit exceeds a critical threshold, this drought resistance behavior can be invalid and can cause degradation and even death of vegetation, and subsequent downstream losses in terrestrial carbon uptake (Fu et al., 2022b; Meir et al., 2015; Meng et al., 2022; Oglesby et al., 2002). However, soil moisture thresholds (SMTs) are still unclear at global scale. Therefore, estimating SMT is crucial to protect terrestrial carbon sinks and to reduce uncertainties in predictions of future terrestrial carbon uptake and climate change.

SMT are usually estimated either by direct observation of the critical threshold when the vegetation characteristics vary significantly or by calculating the inflection points of regression models between vegetation growth

Table 1
Output Variables of Community Earth System Model Version 2

Variables	Units	Long name
GPP	gC m^{-2} $month^{-1}$	Gross primary production
SM	m^3 m^{-3}	Volumetric soil moisture
T	℃	2 m air temperature
RH	%	2 m relative humidity
RAD	W m^{-2}	Atmospheric incident solar radiation
QROOTSINK	mm $month^{-1}$	Water flux from soil to root in each soil-layer

characteristics and their SM status (B. C. Xu et al., 2010; Yan et al., 2017). Typical regression models include logistic regression model (Toms & Villard, 2015), negative exponential regression model (Sadras & Milroy, 1996), quadratic polynomial model (B. C. Xu et al., 2010), plateau regression model (Meir et al., 2015) and linear spline model (Soltani et al., 2000). However, these models still have many limitations in fitting the relationship between GPP and SM, and artificial neural networks offer significant advantages and flexibility in fitting these complex nonlinear relationships (Wang et al., 2015). In addition, the observed samples have usually been quite limited due to the restriction of simulation experiments in the amounts and ranges of soil water gradients, which may not encompass the critical threshold or may be unable to establish a regression model that accurately estimates the critical threshold. A recent study proposed a global critical drought threshold map by considering coupled climate anomaly and vegetation response to drought (Li et al., 2023). While the study advanced the understanding the drought impacts on vegetation in changing climate, the underlying mechanisms were not analyzed. This is because observational data can be affected by many environmental perturbations, and it is very

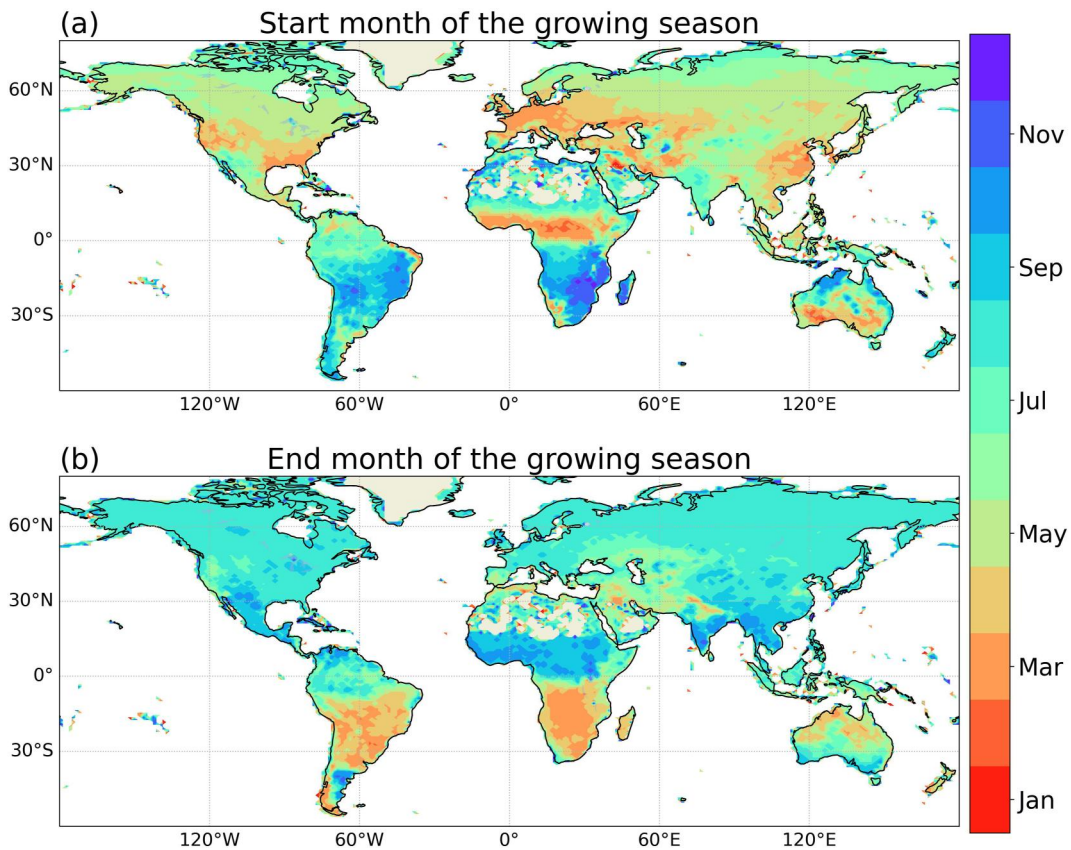

Figure 1. *Global maps of start (a) and end (b) month of the growing season used in this study*. The growing season data set source from Zhang and Henebry (2020). Both are converted from daily to monthly scale and interpolated to the same resolution as experiment REF with nearest neighbor method.

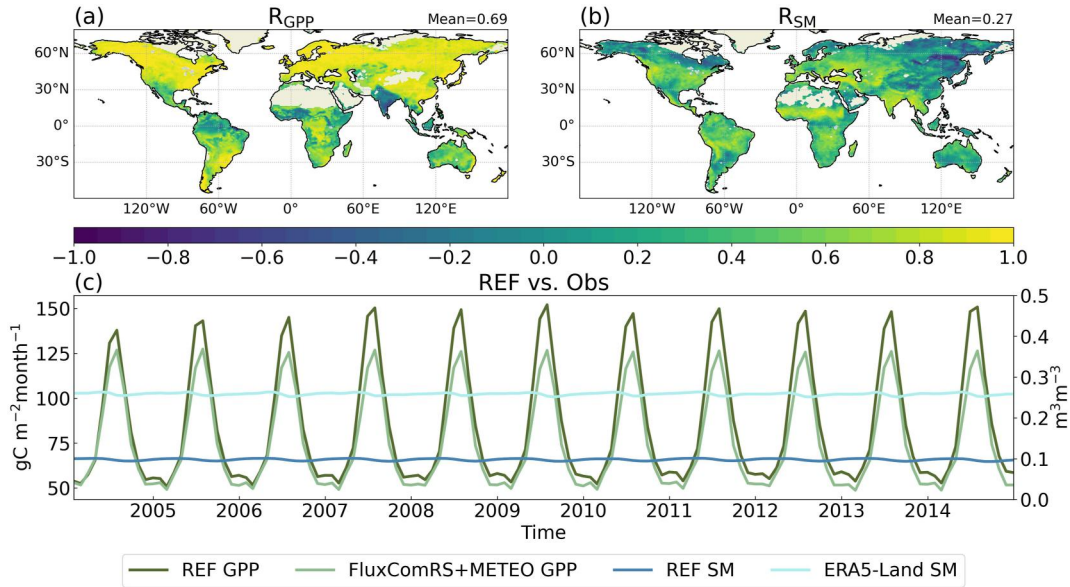

Figure 2. *The spatial patterns of Pearson correlation coefficient (R) and the spatial average interannual variation of gross primary production (GPP) and soil moisture (SM).* (a) The spatial patterns of *R* between REF GPP and FluxComRS + METEO GPP from 2004 to 2014. (b) The spatial patterns of *R* between REF SM and Era5-Land SM from 2004 to 2014. *R* are calculated from monthly data for all months from 2004 to 2014 for each gridcell. The global mean value is displayed at upper right corner. (c) The spatial average interannual variation of REF GPP (dark green), FluxComRS + METEO GPP (light green), REF SM (dark blue) and Era5-Land SM (light blue). The SM axis is on the right, and the GPP axis is on the left. Both of FluxComRS + METEO and Era5-Land are interpolated to the same resolution as experiment REF with bilinear interpolation method.

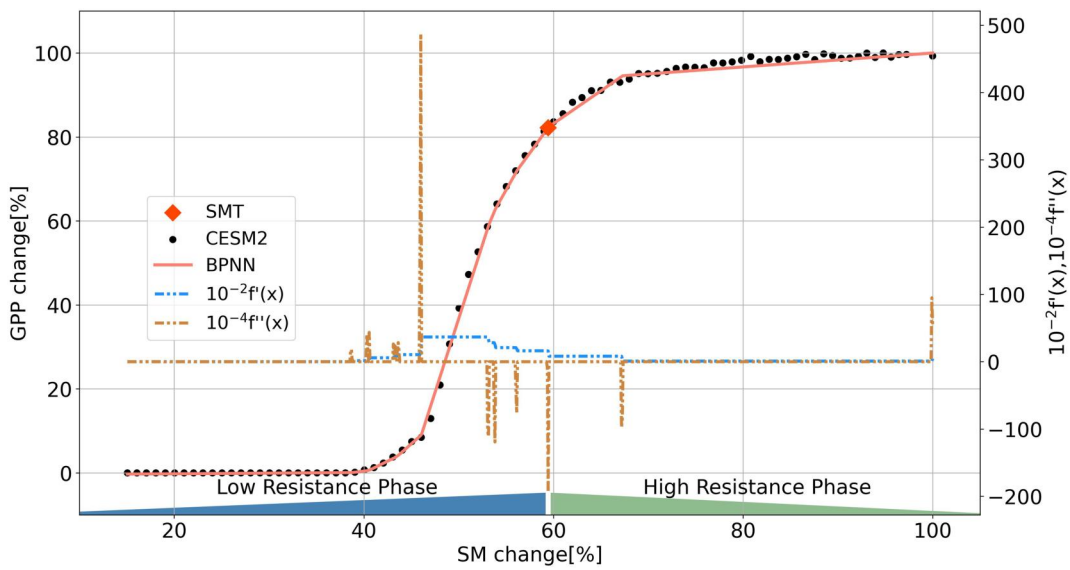

Figure 3. *Comparison between experimental data and back propagation neural network (BPNN) results*. The black dots are gross primary production (GPP) results from 86 experiments. The red line is Artificial Neural Network fitting curve. The blue dash dot line is $10^{-2} f'(x)$. The brown dash dot line is $10^{-4} f''(x)$. The red dot is the soil moisture (SM) threshold (SMT) for aggravating terrestrial carbon uptake losses. SMT is defined as SM with the minimum value of $f''(x)$ when $f'(x) > 0$. Two vegetation response phases are defined: high resistance phase (SM > SMT) and low resistance phase (SM < SMT). The result comes from gridcell where locate at 0° and 60°W. The *x*-axis and *y*-axis are SM change and GPP change relative to normal (experiment REF).

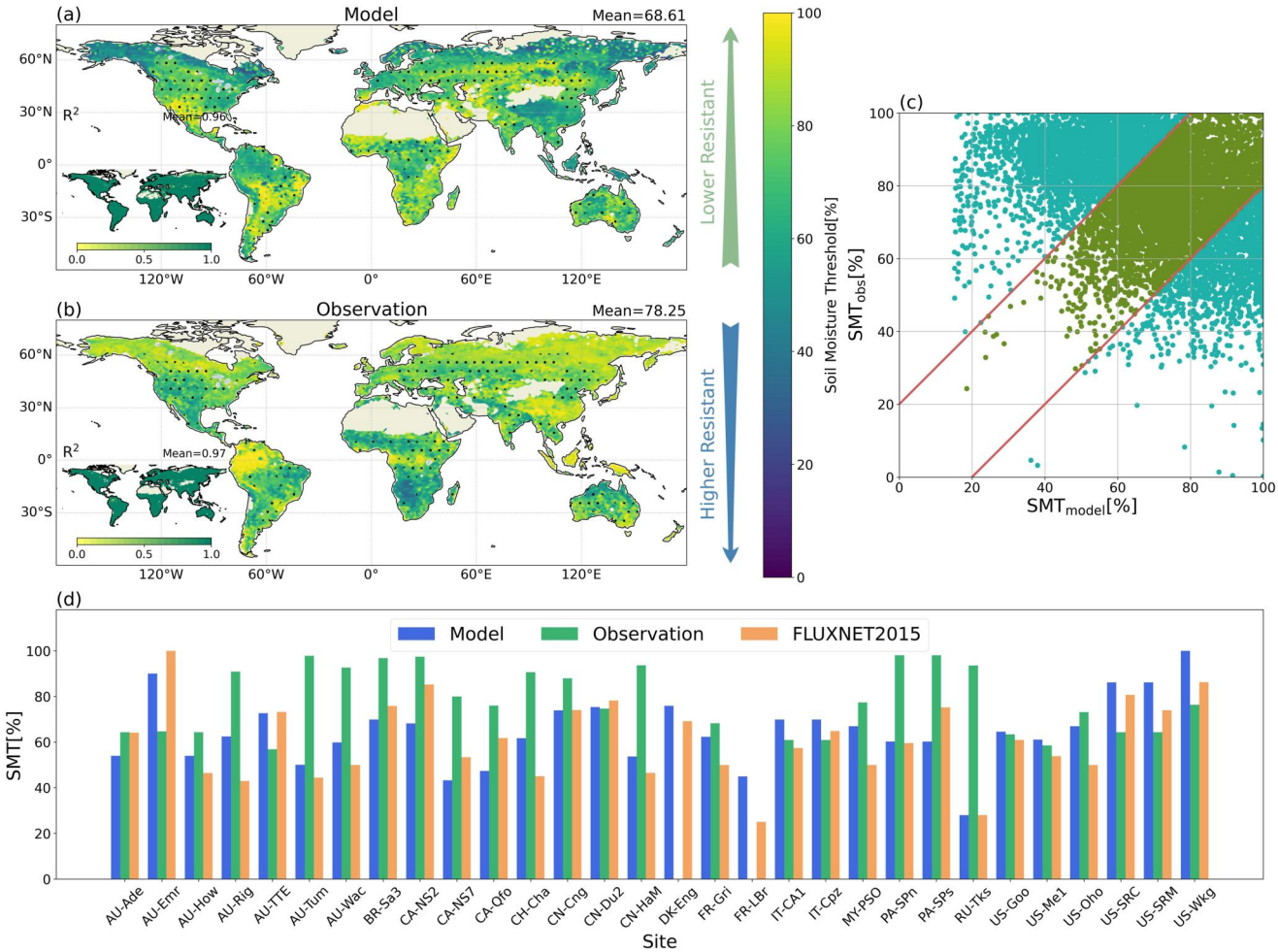

Figure 4. *Global map of soil moisture thresholds (SMT) for aggravating global terrestrial carbon uptake losses*. (a, b) The spatial patterns of SMT from model simulations and observation during 2004–2014. The insets on (a) and (b) show the distributions of goodness of fit (R^2). The global mean value is displayed at upper right corner for (a) and (b) plots and their insets. (c) The quantile-quantile plot for SMT_{model} and SMT_{obs}. The green dots represent the gridcells where SMT_{model} and SMT_{model} differ by less than 20% and these gridcells are marked on (a) and (b) with black dots. (d) 30 sites' SMT was estimated using the FLUXNET2015 data set, observations, and models. All results of SMT are SM change relative to normal.

difficult to separate these environmental perturbations individually. Since SM deficit is likely to continue increasing in frequency and intensity with global warming (L. Xu et al., 2019), determining the response of GPP on SM deficit and SMT is essential for predicting soil drought risk and preparing for future climate change.

After decades of development, the current Earth system models have been able to simulate the changes of global terrestrial carbon uptake and SM (Gentine et al., 2019; Hurk et al., 2016; Santos et al., 2021), and can better reflect the nonlinear relationship between terrestrial carbon uptake and SM (Green et al., 2019). For example, the Community Earth System Model Version 2 (CESM2) is one of the most widely used Earth system models. The influence of soil water on vegetation often represents by a soil water stress factor simply (Rogers et al., 2017), The land surface module of its latest version (The Community Land Model, CLM5) introduced a plant hydraulic stress model of water transport in which vegetation replaces the empirical SM stress equation, which lack either a strong physical or empirical justification and are a major source of uncertainty in the land module (Kennedy et al., 2019; D. M. Lawrence et al., 2019). The plant hydraulic stress routine which explicitly models water transport through the vegetation according to a simple hydraulic framework following Darcy's Law for porous media flow equations. The water stress of vegetation is solved with transpiration demand instead of soil water content in PHS. Therefore, the impact of SM deficit on GPP can be simulated based on physical processes, rather than through empirical equations.

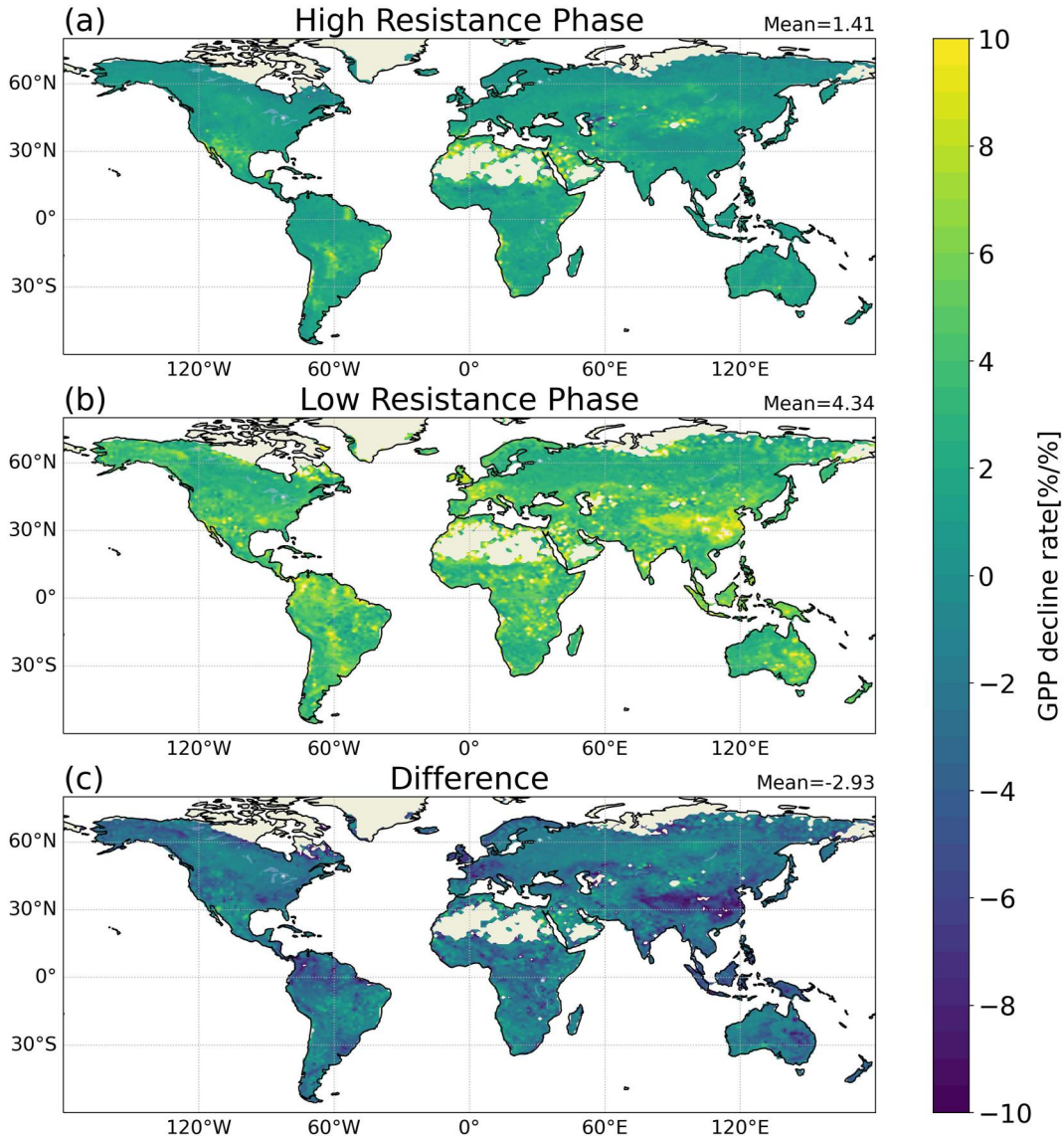

Figure 5. *Global map of gross primary production (GPP) decline rate at high and low resistance phase*. (a, b) The spatial patterns of GPP decline rate at high and low resistance phase during 2004–2014. (c) The difference between (a) and (b) ((a) minus (b)). GPP decline rate is defined as percentage of GPP decline for every 1% decrease in soil moisture relative to normal.

Here, we designed a series of numerical simulations with different SM deficits using CESM2 to investigate the relationship of GPP and SM during the growing seasons from 2004 to 2014. Back propagation neural network (BPNN) is employed to accurately fit the complex nonlinear relationship between GPP and SM and to estimate SMT.

2. Experiments and Methods

2.1. Experimental Setup

CESM version 2.1.3 (CESM2) is employed in this study. CESM2 is an open-source, comprehensive earth system model designed primarily for studies of Earth's past, present, and future climates. It includes ocean, atmosphere, land, sea ice, land-ice, river, and wave model components (Danabasoglu et al., 2020). To more accurately reflect the impact of SM deficit, such as increasing temperature and vapor pressure deficit (VPD) due to SM deficit, we used a coupled land–atmosphere model involving the Community Atmosphere Model 6 (CAM6) and Community

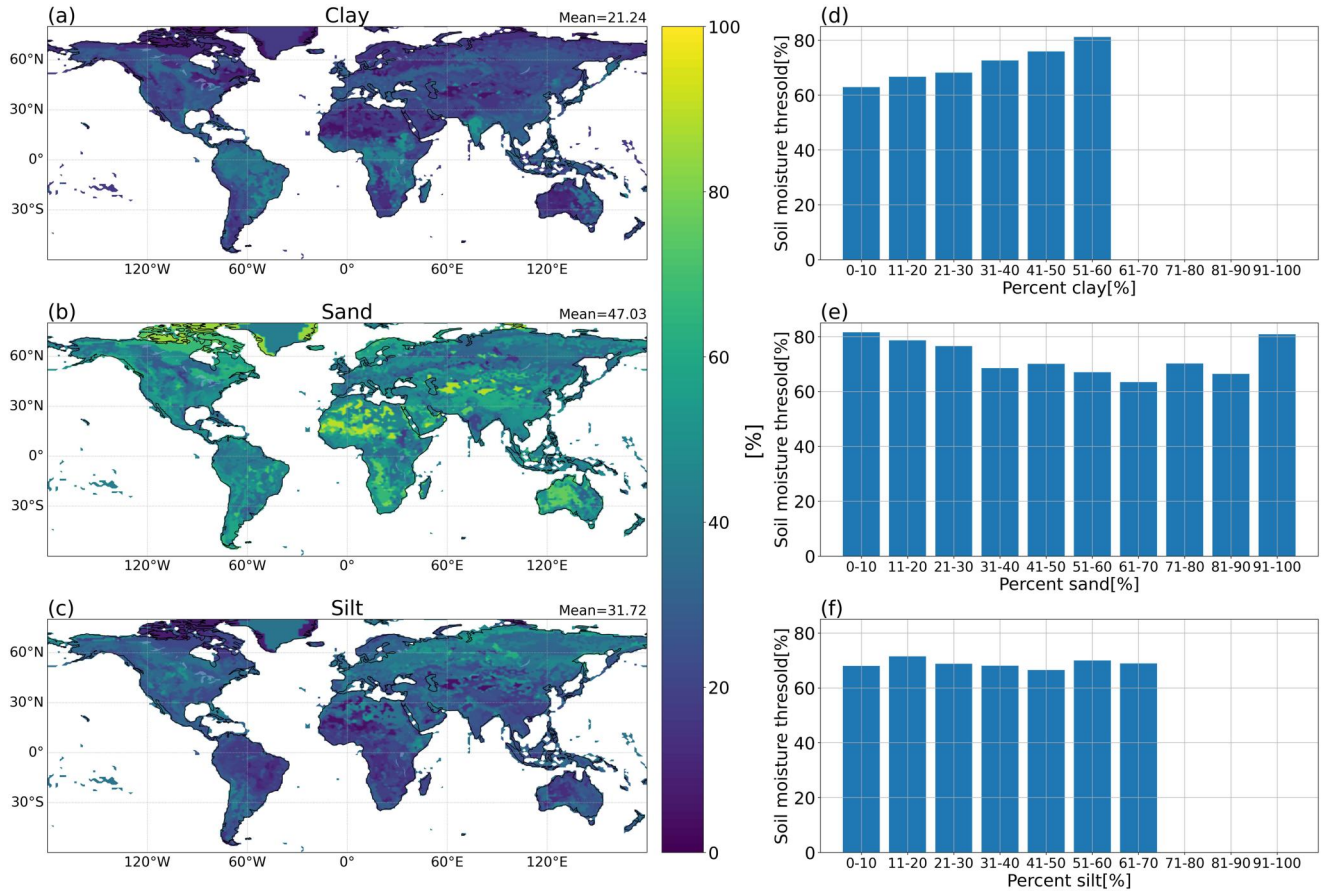

Figure 6. *Characteristics of soil moisture thresholds (SMTs) for different soil texture*. (a–c) The spatial patterns of clay, sand and loam content for 0–3 m soil. (d–f) The average SMT for different clay, sand and loam content. All results of SMT are SM change relative to normal. The soil texture data set source from Bonan et al. (2002). The data set is interpolated to the same resolution as experiment REF with bilinear interpolation method.

Land Model version 5 (CLM5). The coupled model simulates the plant physiology, phenology, growth, and mortality along with the terrestrial water, carbon, and nitrogen cycles, and the soil column can be discretized into 20 hydrologically and biogeochemically active layers (0–8.6 m) (Oleson et al., 2013). Sea surface temperature and sea ice are prescribed as 2000 years to eliminate the influence of the ocean.

Here, we run 86 numerical simulations, including one reference experiment (REF) and 85 perturbation experiments (EXP_n). Pre-simulation is the same initial simulation used by CESM2 in the Land Surface, Snow and SM Model Intercomparison Project (Hurk et al., 2016). Land surface data with a spatial resolution of 1° over global is generated using the tool provided by CLM5. First, we run a default land-atmosphere couple reference experiment with the output monthly SM. Second, 85 perturbation experiments which all configurations are the same as REF except SM are carried out. The output of SM from REF is used as the input to EXP_n. The SM is altered at each month as:

$$SM_{EXP_n} = SM_{REF}\left(1 - \frac{n}{100}\right), n = 1,2,3\ldots\ldots,85 \quad (1)$$

where n is the percentage of decrease in SM relative to REF and SM_{REF} is the SM of REF output. Since the water balance in CESM2 is difficult to maintain when SM deficit >85% and extreme droughts like this are very rare, n is restricted to <85%.

Table 2
Classifications of Climate Zone Reclassify From Beck et al. (2020)

Köppen-Geiger climate zones	Reclassified climate zones
Tropical, rainforest	Tropical
Tropical, monsoon	
Tropical, savannah	
Arid, desert, hot	Arid
Arid, desert, cold	
Arid, steppe, cold	
Arid, steppe, hot	
Temperate, dry summer, hot summer	Temperate
Temperate, dry summer, hot summer	
Temperate, dry summer, cold summer	
Temperate, dry winter, hot summer	
Temperate, dry winter, warm summer	
Temperate, dry winter, cold summer	
Temperate, no dry season, hot summer	
Temperate, no dry season, warm summer	
Temperate, no dry season, cold summer	
Cold, dry summer, hot summer	Cold
Cold, dry summer, warm summer	
Cold, dry summer, cold summer	
Cold, dry summer, very cold winter	
Cold, dry winter, hot summer	
Cold, dry winter, warm summer	
Cold, dry winter, cold summer	
Cold, dry winter, very cold winter	
Cold, no dry season, hot summer	
Cold, no dry season, warm summer	
Cold, no dry season, cold summer	
Cold, no dry season, very cold winter	
Polar, tundra	X
Polar, frost	

Note. Thirty-five climate zones are reclassified into four climate zones. The symbol X means this climate zone is excluded because of its low GPP and vegetation coverage rate.

The output variables of CESM2 include GPP, SM, 2 m air temperature, 2 m relative humidity, atmospheric incident solar radiation and water flux from soil to root (Table 1). Two meter temperature and relative humidity are used to calculate VPD with the eighth-order polynomial fits (Flatau et al., 1992). All experiments covered the period from 2004 to 2014. Resolution of both land and atmosphere models are longitude 1.25° and latitude 0.9°. For global analysis and plot, output data of the growing season (Figure 1; Zhang & Henebry, 2020) from 2004 to 2014 are selected because the relationship between SM and GPP is strongest during growing seasons. All data are interpolated to the same resolution as experiment REF with majority interpolation methods. Instead of whole soil depth (from 0 to 8.6 m in CLM5), SM is measured as average volumetric soil water content (percentage) from 0 to 3 m, where SM interacts mostly with the atmosphere and vegetation.

Monthly observed GPP and SM are used to validate model performances, We obtained the observed 2004–2014 monthly GPP from FluxComRS + METEO data set (Jung et al., 2019, 2020). FluxComRS + METEO uses machine learning to merge carbon flux measurements from eddy covariance towers with remote sensing and meteorological data to estimate GPP. We also used the observed 2004–2014 monthly SM from Era5-Land to validate model performances (Munoz, 2019; Munoz et al., 2021). Era5-Land provides volume of water in soil layer (0–2.89 m) of the European Centre for Medium-Range Weather Forecasts Integrated Forecasting System. Although SM provided by Era5-Land is little shallower than CESM2, the validation requirements of this study are met because their depths are close. Both of FluxComRS + METEO and Era5-Land are interpolated to the same resolution as experiment REF with bilinear interpolation method.

2.2. Estimation of Soil Moisture Thresholds

Based on the experiments above, SMT are defined as the inflection point at which vegetation transitions from high to low drought resistance. We provide a method that fits the nonlinear relationship of GPP and SM with BPNN, and SMT can be estimated in a systematic fashion. BPNN is widely recognized as an artificial neural networks for predictive and pattern recognition cases. Different from parametric equations, BPNN's outstanding advantages are strong nonlinear mapping ability and flexible network structure (Wang et al., 2015).

The details of the estimation procedure are described below:

(1) GPP and SM are selected for each experiment based on start and end months of growing seasons (Figure 1) from the monthly data during 2004–2014. The selected data are then averaged over time.
(2) For all experiments, all averaged GPP and SM are reassembled into a new data set in order of SM from lowest to highest (a $N_{exp} \times N_{lat} \times N_{lon}$ vector, where $N_{exp} = 86$, N_{lat} and N_{lon} are the gird number of zonal and meridional direction).
(3) For reassembled data, BPNN is constructed to fit the nonlinear relationship of GPP and SM. The ability of BPNN to handle actual problems is determined by its network structure (Shao, 2009). The fitting accuracy of BPNN can theoretically increase with more hidden layers and neurons. In this study, in order to balance the complexity of BPNN and fitting results, the hidden layer is set to 3 and the number neurons in each layer is set to 100. The number of input layer nodes and output layer nodes is set to 1. The selection of the activation function is related to the final optimization result (Tian et al., 2022). This study selects the piecewise linear rectification function Relu as the activation function of the neural network. Because BPNN is not a prediction

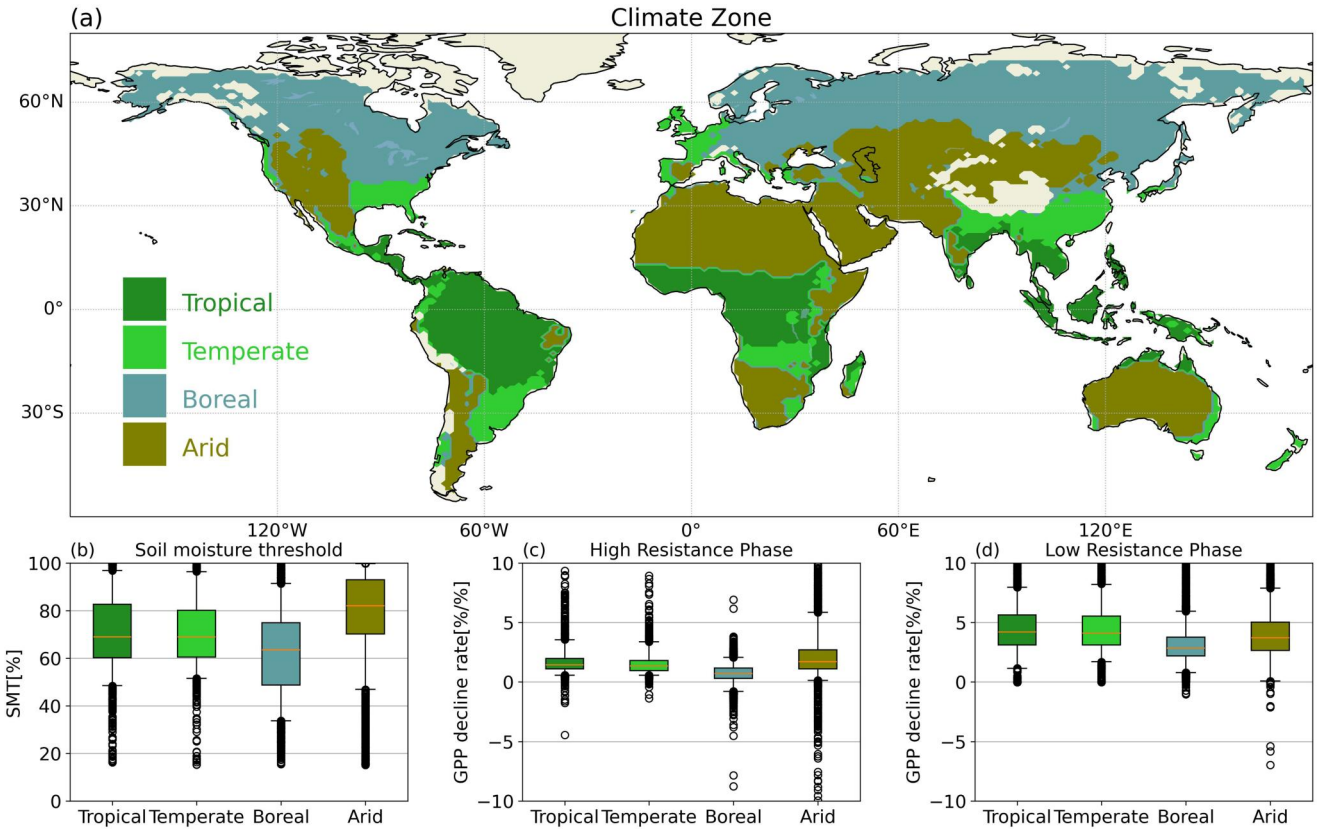

Figure 7. *Characteristics of soil moisture thresholds (SMTs) for different climatic zones*. (a) The spatial patterns of climate zones. The climate zones data set from Beck et al. (2020) is reclassified to make it suitable for this study (Table 2). (b) The SM thresholds for four climate zones. The SMT are SM change relative to normal. (c, d) The gross primary production decline rate for four climate zones during high and low resistance phase.

Table 3
Soil Moisture Thresholds of 14 Vegetation Types

Vegetation type	Acronym	Soil moisture threshold (%)
Needleleaf evergreen tree—temperate	NET Temperate	68.21
Needleleaf evergreen tree—boreal	NET Boreal	72.63
Needleleaf deciduous tree—boreal	NDT Boreal	57.21
Broadleaf evergreen tree—tropical	BET Tropical	56.41
Broadleaf evergreen tree—temperate	BET Temperate	73.16
Broadleaf deciduous tree—tropical	BDT Tropical	74.45
Broadleaf deciduous tree—temperate	BDT Temperate	72.87
Broadleaf deciduous tree—boreal	BDT Boreal	73.22
Broadleaf evergreen shrub—temperate	BES Temperate	59.21
Broadleaf deciduous shrub—temperate	BDS Temperate	79.44
Broadleaf deciduous shrub—boreal	BDS Boreal	75.86
C3 arctic grass		54.74
C3 non-arctic grass		54.78
C4 grass		73.76

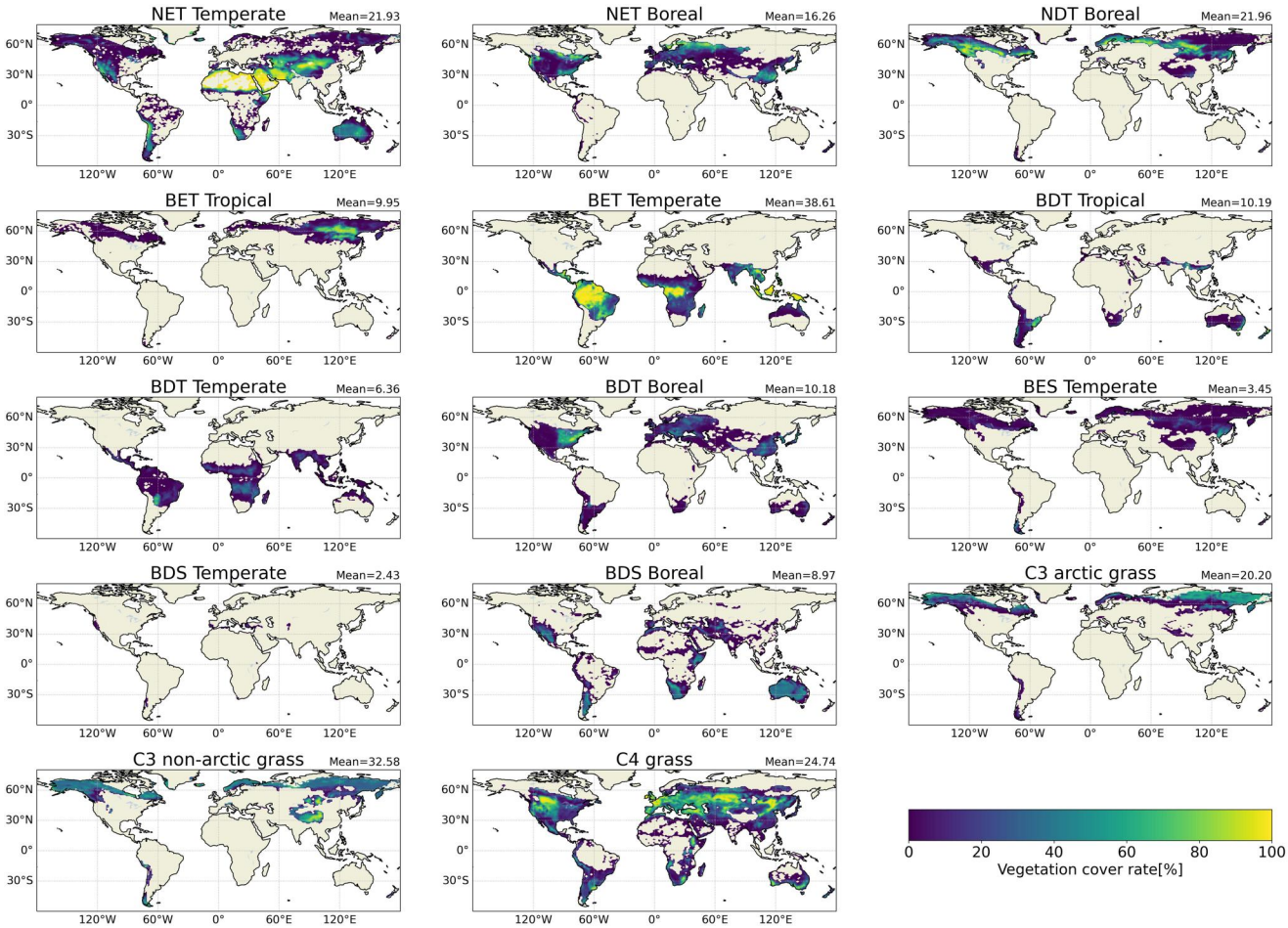

Figure 8. *Global map of 14 possible vegetation types distribution and their coverage rates*. Table 3 shows the detailed information for each vegetation type. Community Land Model version 5 revealed that these plant types differ in root distribution parameters that control the uptake of water from the soil; aerodynamic parameters that determine resistance to heat, moisture, and momentum transfer; and photosynthetic parameters that determine stomatal resistance, photosynthesis, and transpiration. The vegetation coverage rate data set source from P. J. Lawrence and Chase (2007). The data set is interpolated to the same resolution as experiment REF with bilinear interpolation method.

model in this study, all experiments' data from each gridcell are used for training. BPNN performances are evaluated by goodness of fit (R^2).

$$\mathrm{GPP} = \mathrm{BPNN}(\mathrm{SM}) \tag{2}$$

(4) SMT is defined as SM with the minimum value of $f''(x)$ at each gridcell when $f'(x) > 0$. Here $f(x)$ represents the curve-fitting result of BPNN. $f'(x)$ and $f''(x)$ is the first and second derivatives. $f'(x) > 0$ is to ensure that the relationship between GPP and SM is monotonically increasing. $f''(x)$ takes the minimum value to represent GPP decline rate varies most when SM decreases.

(5) SMT distinguishes two vegetative drought response phases: high and low resistance phases. The transformation for high to low resistance phase implies vegetation adjusts from a rapid to a slow carbon uptake rate. Vegetation become more sensitive to SM deficit at low resistance phase. Average decline rates of GPP are estimated by the first derivative of $f(x)$ during high and low resistance phases.

This estimation procedure is also applied to FluxComRS + METEO and Era5-Land data set. Different from experiment data, we use 2004–2014 monthly data of them as BPNN input to ensure there are enough training samples. We also used daily FLUXNET2015 site data as another data set to validate SMT (Pastorello et al., 2020). The evaporative fraction-soil moisture method was applied to estimate SMT on site level (Fu

Table 4
30 FLUXNET2015 Sites Used in This Study

SITE ID	_LAT	LONG	PFT	Periods
AU-Ade	−13.0769	131.1178	WSA	2007–2009
AU-Emr	−23.8587	148.4746	GRA	2011–2013
AU-How	−12.4943	131.1523	WSA	2001–2014
AU-Rig	−36.6499	145.5759	GRA	2011–2014
AU-TTE	−22.287	133.64	GRA	2012–2014
AU-Tum	−35.6566	148.1517	EBF	2001–2014
AU-Wac	−37.4259	145.1878	EBF	2005–2008
BR-Sa3	−3.018	−54.9714	EBF	2000–2004
CA-NS2	55.9058	−98.5247	ENF	2001–2005
CA-NS7	56.6358	−99.9483	OSH	2002–2005
CA-Qfo	49.6925	−74.3421	ENF	2003–2010
CH-Cha	47.2102	8.4104	GRA	2005–2014
CN-Cng	44.5934	123.5092	GRA	2007–2010
CN-Du2	42.0467	116.2836	GRA	2006–2008
CN-HaM	37.37	101.18	GRA	2002–2004
DK-Eng	55.6905	12.1918	GRA	2005–2008
FR-Gri	48.8442	1.9519	CRO	2004–2014
FR-LBr	44.7171	−0.7693	ENF	1996–2008
IT-CA1	42.3804	12.0266	DBF	2011–2014
IT-Cpz	41.7052	12.3761	EBF	1997–2009
MY-PSO	2.973	102.3062	EBF	2003–2009
PA-SPn	9.3181	−79.6346	DBF	2007–2009
PA-SPs	9.3138	−79.6314	GRA	2007–2009
RU-Tks	71.5943	128.8878	GRA	2010–2014
US-Goo	34.2547	−89.8735	GRA	2002–2006
US-Me1	44.5794	−121.5	ENF	2004–2005
US-Oho	41.5545	−83.8438	DBF	2004–2013
US-SRC	31.9083	−110.8395	OSH	2008–2014
US-SRM	31.8214	−110.8661	WSA	2004–2014
US-Wkg	31.7365	−109.9419	GRA	2004–2014

Note. SITE ID, Site identifier; LAT, °, latitude; LONG, °, longitude; PFT, plant functional type and study periods are listed. Plant functional types were defined according to the IGBP classification, including ENF, evergreen needleleaf forests; EBF, evergreen broadleaf forests; DBF, deciduous broadleaf forests; GRA, grasslands; CRO, croplands; OSH, open shrublands; WSA, woody savannas.

et al., 2022a). There are 30 sites with SMT estimates using first SM measurement depth. The detail information of 30 sites can be found in Table 4.

2.3. Sensitivities of GPP to SM, VPD, and *T*

Following previous studies (Dannenberg et al., 2022; Fu et al., 2022b), monthly time series of GPP, SM, VPD, temperature (T), and atmospheric incident solar radiation (RAD) are normalized (z-scores) to derive the standardized sensitivity of GPP to SM, VPD, T and RAD. For each variable, the monthly data from 2004 to 2014 are used to ensure sufficient samples.

We generated the spatial average for each variable in each experiment, normalized the average data, and then used ridge regression (Park, 2017) to estimate monthly GPP sensitivities to SM, VPD, and T from 2004 to 2014. Ridge regression is employed to exclude the collinearity between SM, VPD and T.

$$\mathrm{GPP} = \beta_1 \mathrm{SM} + \beta_2 \mathrm{VPD} + \beta_3 T + \beta_4 \mathrm{RAD} + b + \varepsilon \quad (3)$$

where β_i is the standardized sensitivity of GPP to each variable, b represents the intercept, and ε is the random error term. We compared sensitivities to quantify the impact of SM and land-atmosphere feedback on terrestrial carbon uptake.

3. Results

3.1. Model Verification

All the perturbation experiments are based on the REF experiment. Thus, the results of the REF experiment directly affect the accuracy of our results. In particular, GPP and SM are considered to estimate the impact of SM deficit on terrestrial carbon uptake. The Pearson correlation coefficient (R) of REF and FluxComRS + METEO is calculated using monthly GPP data from 2004 to 2014 (Figure 2a). CESM2 performs well in GPP simulation at the regions north of 30°N but poorly near the equator. CESM2 performs poorly in SM simulation and may be the most significant source of uncertainty in SMT estimation (Figure 2b) (Trugman et al., 2018). We also compared the spatial average interannual variations of GPP and SM with observation data (Figure 2c). The result shows that CESM2 can simulate the season cycle of GPP while underestimate the SM.

3.2. Global Distribution of Soil Moisture Thresholds

Figure 3 shows the comparison of experimental and BPNN results at 0° and 60°W. Here SMT is estimated to be 59.44% relative to normal (experiment REF). GPP decline rate is defined as percentage of GPP decline for every 1% decrease in SM relative to normal. The GPP decline rate is 0.44%/% and 5.44%/% at the high and low resistance phases. The GPP decline rate is amplified by a factor of 12.4. The results show that global terrestrial carbon uptake losses will worsen once the SM deficit exceeds SMT.

We also demonstrate that SMT varies geographically around the globe characterized by higher SMTs in SM-limited than in energy-limited ecoregions. We find that SMT from the model occurs at values >70% of SM anomalies in 49% of regions (Figure 4a). This suggests that terrestrial carbon uptake losses are likely to being aggravated when SM deficit exceeds 30% relative to the normal value in half the regions. Although local consistent between neighboring points, our model-based SMT have strongly geographical variation. For region where have higher SMT, lower levels of SM stress can induce a vegetation response to drought. This lower

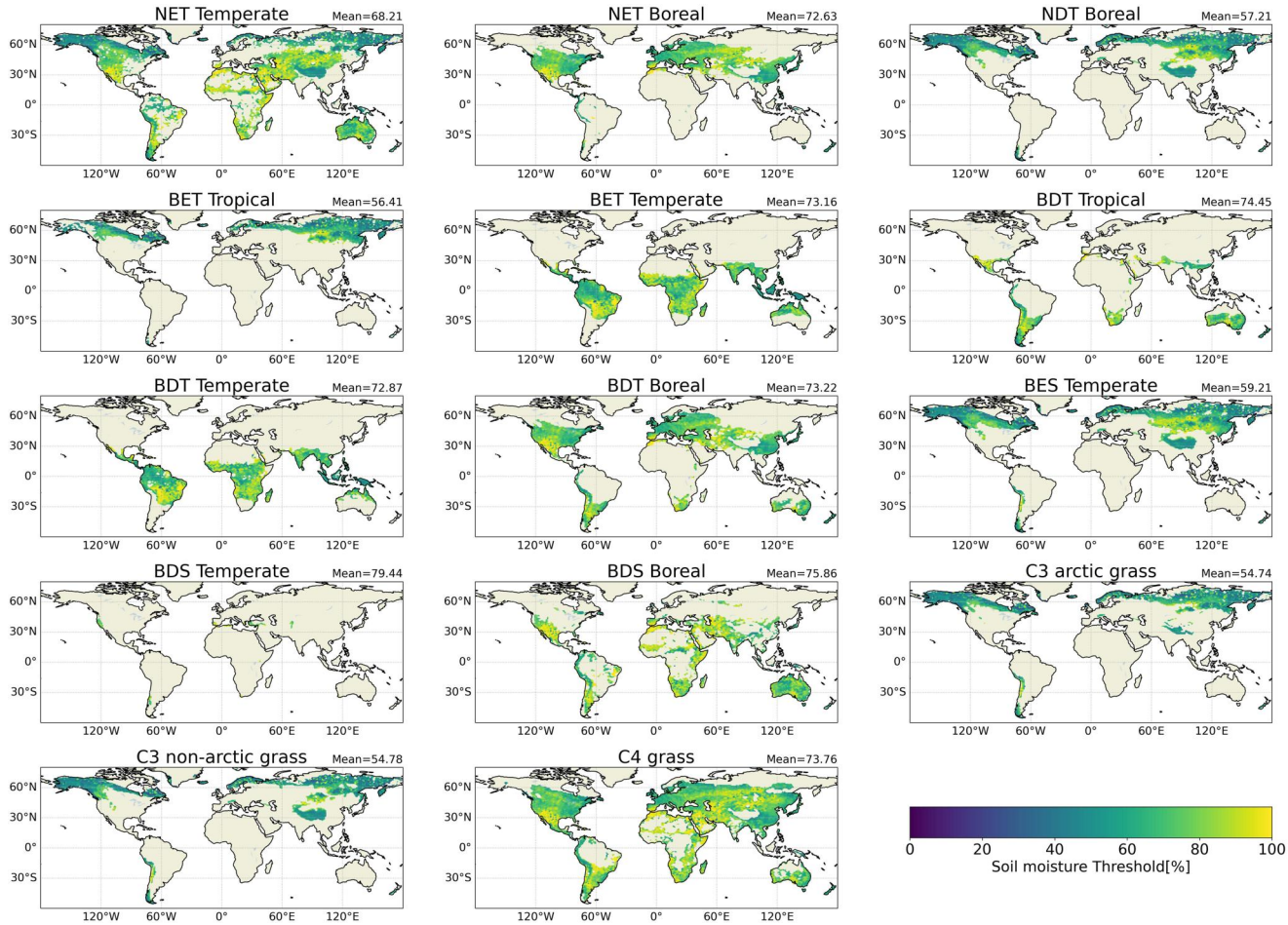

Figure 9. *Global map of soil moisture threshold (SMT) of 14 possible vegetation types*. The SMT are SM change relative to normal.

resistance corresponds to a vulnerable capacity for vegetation to mitigate SM deficit and reduce sensitivity to drought. These regions are more vulnerable to drought and leads to the degradation and death of vegetation. SMT are also estimated using observed data (Figure 4b). By contrast, observed-based SMT are higher than model-based SMT in most regions. Drought in the natural environment is frequently accompanied by an increase in pests, illnesses, and fires, which is more likely to aggravate terrestrial carbon uptake losses than model simulation. The difference is most noticeable in forested areas, such as Amazon, southern USA and southern China. Figure 4c reveals 50.35% of the regions have less than 20% difference between observed-based SMT and model-based SMT. A comparison of model, observation and FLUXNET2015 at site level is displayed in Figure 4. The correlation between the model and FLUXNET2015 is 0.79, and the root mean square error of SMT between the two is 11.2%.

The global mean GPP decline rate is 1.41%/% during high resistance phase while 4.34%/% during low resistance phase (Figure 5). Vegetation will be more sensitivity to drought in low resistance phase than in high resistance phase. Terrestrial carbon uptake losses rate is magnified by a factor about 3 on a global scale, particularly in Amazon and southern China where forest coverage rate is high (Figure 5c). Generally, model-based SMT have a more valid and stronger association with soil texture, climate zones, vegetation type and vegetation coverage rate.

The water retention curves of varied soil textures can change the spatial distribution of SMT. The soil texture data set sourcing from Bonan et al. (2002) is used to analyze the characteristics of SMT under various soil texture (Figure 6). SMT have a strong positive link with clay content while a negative correlation with sand content. Soil moisture increases gradually as clay content increases and sand content decreases under the same matrix suction (C. Yang et al., 2023). The regions where have higher clay content typically have wetter soil. These humid regions

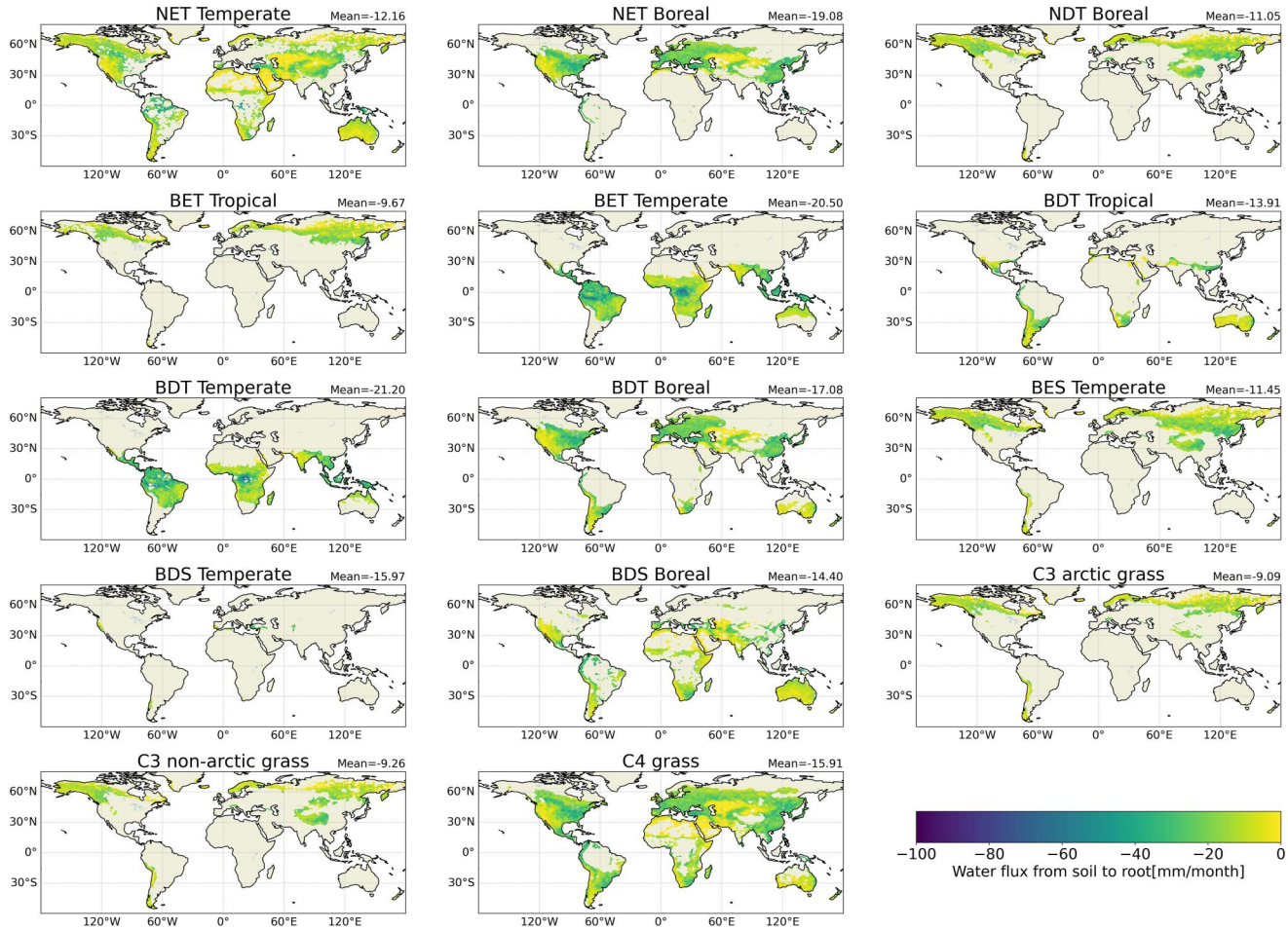

Figure 10. *Global map of water flux difference from soil (0–3 m) to root for 14 possible vegetation types relative during high and low resistance phases*. The change is calculated by water flux during low resistance phase minus water flux during high resistance phase for each vegetation type.

are theoretically more sensitive to drought (C. Yang et al., 2023), leading to higher SMT are detected. There is no discernible relationship between SMT and silt content.

For climate zones, Beck et al. (2020) presented a new global map of the Köppen-Geiger climate classification at an unprecedented 1 km resolution for the present day. Here, we reclassified the 30 climate zones for growing seasons and resampled the data to make them suitable for our study (Table 2, Figure 7a). SMT are highest in dry zones (79.03%), followed by tropical (70.67%) and temperate zones (70.50%). SMT are lowest in the boreal zones, with 62.21% (Figure 7b). Only the temperate zone's SMT is near to the tropic. The vast majority of population resides in temperate zones (Cohen & Small, 1998), anthropogenic activities that include agricultural management and land use change have reduced carbon losses, even though there are less water in temperate zone (Wu & Wu, 2023). The GPP decline rate of arid zones is higher than that of the other three climate zones at high resistance phase (tropical: 1.67%/%; temperate: 1.55%/%, boreal: 0.71%/%; arid: 2.06%/%). In other words, arid zones may be stressed first in a future climate characterized by an increased frequency, intensity, duration and extent of extreme drought events. However, during low resistance phase, the GPP decline rate of tropical and temperate zones are higher than boreal and arid zones (tropical: 4.40%/%; temperate: 4.41%/%, boreal: 3.09%/%; arid: 3.90%/%). This result shows that when SM deficit exceeds SMT, tropical and temperate zones will experience higher terrestrial carbon uptake losses than boreal and arid zone.

SMT display a more valid and stronger association with vegetation types. Surfaces covered by vegetation can have up to 14 possible vegetation types in CESM2 (Table 3, Figure 8; P. J. Lawrence & Chase, 2007). These vegetation types differ in root distribution parameters that control the uptake of water from soil; aerodynamic

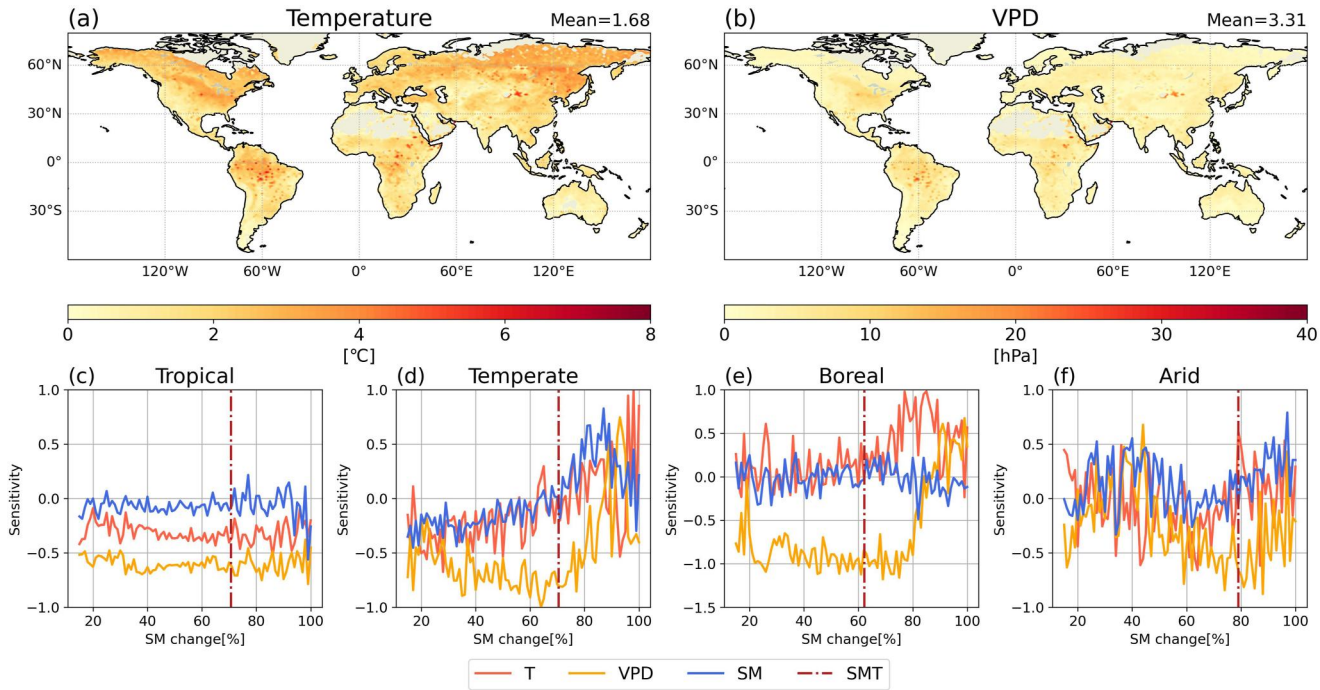

Figure 11. *Impact of soil moisture (SM) deficit on land–atmosphere*. (a, b) Difference between 2 m air temperature and vapor pressure deficit (VPD) during low and high resistance phases (low phase minus high phase). (c–f) The sensitivity of gross primary production to temperature (T) (red), VPD (orange) and SM (blue). The red dash line represents the average SM threshold of four climate zones.

parameters that determine resistance to heat, moisture and momentum transfer; and photosynthetic parameters that determine stomatal resistance, photosynthesis and transpiration. We extracted SMT of 14 vegetation types and calculated their average SMT (Figure 9). Because of its limited coverage area, the broadleaf deciduous shrub Temperate result is excluded from the analysis. Broadleaf deciduous tree (BDT) Tropical have the highest SMT (74.45%) while C3 arctic grasses have the lowest SMT (54.74%). BDT Tropical is commonly found north and south of tropical rainforests, as well as in dry land areas south or north of subtropical deserts. These areas have long dry seasons that can last for months and are extremely sensitive to SM deficit, which can easily reach a threshold and drastically alter natural communities. Generally speaking, SMT in forested ecosystems is related to vegetation coverage rate (Figures 8 and 9). The higher the vegetation coverage rate and the humid climate, the lower the SMT and the less sensitive to SM deficit. The SMT of C4 grasses are close to the majority of forests. The SMT of C3 grasses are substantially lower than forests, indicating that C3 grasses have greater adaptation when severe drought occurs. Planting C3 grasses may be more effective and cost-effective than planting trees and C3 grasses in enhancing the ecology of some arid ecoregions.

To understand the influence of vegetation roots on SMT, we examined the water flux from soil to root for different vegetation types (Figure 10). Forests are regarded to be more drought resistant than shrubs and grasslands commonly because they may store more water and acquire water from deeper soil layers when the shallow soil dries due to changes in woody structures and root distribution. However, forests absorb less soil water than vegetation with shallower roots when soil deficit arises in deep soil, for example, SM in the 0–8.6 m soil column is altered in our tests, resulting in a deep SM deficit in this region. Deep soil dryness is more detrimental to forests according to these findings.

3.3. Impact of Land–Atmosphere Feedback on Terrestrial Carbon Uptake

SM deficit can cause decreased evapotranspiration and thus an increase in temperature and VPD. SM deficit is superimposed on a hotter and drier atmospheric background climate (Zhou et al., 2019), which has the potential to significantly aggravate the effects of drought on ecosystems (Grossiord et al., 2020). In other words, land-atmosphere feedback cause by SM deficit is important in aggravating global terrestrial carbon uptake losses. On the one hand, SM deficit can enhance VPD, which may further reinforce stomatal closure of vegetation, restricting the gas exchange between vegetation and the environment and preventing vegetation from absorbing

carbon dioxide (Sulman et al., 2016). In fact, higher VPD due to SM deficit magnify the loss in GPP, accounting for approximately 40% of the GPP anomaly (Dannenberg et al., 2022). On the other hand, SM deficit can result in insufficient evapotranspiration, increasing temperature, changing the activities of enzymes in plants, and negatively influencing photosynthesis, respiration, and other physiological processes of vegetation (Vogel et al., 2017).

A comparison of the 2 m air temperature and VPD during high and low resistance phases revealed that a land–atmosphere feedback SM deficit can raise temperature and VPD. The findings imply that vegetation will endure more severe heat and water stress (Figures 11a and 11b). We computed the sensitivity of GPP to SM, temperature, and VPD for four climate zones based on experiment results (Figures 11c–11f). GPP is more sensitive to SM in tropical zones, followed by temperature and VPD. Guan et al. (2015) put forward that water availability exerts a first-order constraint on vegetation seasonality in tropical forests worldwide. In temperate zones, GPP is more sensitive to SM and temperature when SM > SMT. As SM decrease, the sensitivity of GPP to SM and temperature decreases rapidly and the sensitivity to VPD increases slightly. The result reveal that temperate zone vegetations are governed by SM and temperature at the same time, and that they are more vulnerable in the face of high temperatures and dryness. GPP of boreal zones are sensitive to SM, VPD and temperature when SM > SMT. However, the sensitivity to VPD immediately declines when SM < SMT. The vegetation in the boreal zone is mainly coniferous forest, and their leaves are resistant to VPD due to cold and dry climate. The sensitivity of GPP to SM, VPD, and temperature in arid zones is complex, with GPP being more responsive to SM. In summary, land-atmosphere feedback caused by SM deficit shows a noteworthy shift when SM reach SMT and has a significant limitation on terrestrial carbon uptake.

4. Conclusions and Discussions

In this study, we estimated SMTs for the aggravation of global terrestrial carbon uptake losses using a series of numerical simulations and BPNN. The major results are summarized as follows:

First, global SMTs vary geographically depending on the soil textures, climate zones, vegetation types, and vegetation coverage rate. The spatial distribution of SMTs can be varied by the water retention curves of different soil textures and exhibit a negative association with sand content and a positive association with clay content. Ecoregions that are limited by SM, such as arid zones, have higher SMTs than ecoregions that are limited by energy. Although humid ecosystems, such as tropical rainforests, are less affected by increased vegetation cover, their GPP decline rate is higher than other regions at low resistance phase. This conclusion indicates that terrestrial carbon uptake losses in tropical will be larger than in arid zones when SM lower than SMTs. Moreover, C3 grasses have a significantly lower threshold than forests, suggesting that they are more adapted to periods of extreme dryness. We also found that deep soil dryness is more detrimental to forests by examined the water flux from soil to root for different vegetation types.

Second, the sensitivity of land-atmosphere feedback to GPP varies greatly in different climate zones. Land-atmosphere feedback caused by SM deficit shows a notable change when SM reaches thresholds and has a significant limitation on terrestrial carbon uptake, which may be one of the main reasons for the aggravation of vegetation carbon uptake losses. Our study provides a unique perspective for investigating the impact of drought on vegetation. Understanding and quantifying the responses of GPP to SM deficit is critical for managing ecosystem soil drought risk and reliably projecting terrestrial carbon uptake in the context of global warming.

Although previous studies have estimate SMTs by various kinds of regression models, our study develops a new method of estimating SMTs by integrating a model earth system model and an artificial neural network. In contrast to previous studies, we employ models for simulation because physical process-based models provide a clearer description of numerous key land surface processes than observed data does. In the meanwhile, we use BPNN which fits complex nonlinear circumstances better than parametric models to research the relationship of GPP and SM. However, our study still has several limitations. With the implementation of a plant hydraulic stress function in CLM5.0, GPP should be limited by the interaction of various climate factors rather than just SM, such as CO_2 concentration, precipitation, temperature, humidity. These factors require further investigation and analysis. CESM2 performs poorly in SM simulation and may be the most significant source of uncertainty in SMT estimation. The further studies should be focused on multiple models and finer resolution simulations to reduce the uncertainty caused by single model at different regions. This requires more effort in model development and

simulation. At the watershed scale, more estimation of SMTs ought to be done. The prediction of SMT is also a key point for protecting terrestrial carbon sinks and reducing uncertainties in predictions of future terrestrial carbon uptake and climate change. Moreover, the underestimation of SMTs demonstrates that model shortcomings in representing key land surface processes such as plant and soil hydraulics and unsaturated and saturated lateral flow of soil water. The explicit implementation of these processes to earth system model is essential for improving future climate projections, especially considering the increased frequency of droughts.

Data Availability Statement

CEMS2 Model version 2.1 is provided by NCAR (2018b). The growing season data set from the NASA Visible Infrared Imaging Radiometer Suite (VIIRS) Global Land Surface Phenology (GLSP) product (Zhang & Henebry, 2020). FluxComRS + METEO are provided by Jung et al. (2019). Era5-Land are provided by Munoz (2019). FLUXNET2015 are provided by Pastorello et al. (2020). The climate zone data are provided by Beck et al. (2020). The data of 14 possible vegetation types distribution and soil texture are available at NCAR (2018a). Data used in the figures and analysis in this study is available at Yanheng (2024).

Acknowledgments
This work was supported by the National Natural Science Foundation of China (NSFC) project (Grant 41830967 and 42175163, 42205168) and the National Key Scientific and Technological Infrastructure project "Earth System Science Numerical Simulator Facility" (EarthLab).

References

Beck, H. E., Zimmermann, N. E., McVicar, T. R., Vergopolan, N., Berg, A., & Wood, E. F. (2020). Present and future Koppen-Geiger climate classification maps at 1-km resolution [Dataset]. Scientific Data, *7*(1), 274. https://doi.org/10.1038/s41597-020-00616-w

Bonan, G. B., Levis, S., Kergoat, L., & Oleson, K. W. (2002). Landscapes as patches of plant functional types: An integrating concept for climate and ecosystem models. *Global Biogeochemical Cycles*, *16*(2), 5-1–5-23. https://doi.org/10.1029/2000gb001360

Breshears, D. D., Cobb, N. S., Rich, P. M., Price, K. P., Allen, C. D., Balice, R. G., et al. (2005). Regional vegetation die-off in response to global-change-type drought. *Proceedings of the National Academy of Sciences of the United States of America*, *102*(42), 15144–15148. https://doi.org/10.1073/pnas.0505734102

Cohen, J. E., & Small, C. (1998). Hypsographic demography: The distribution of human population by altitude. *Proceedings of the National Academy of Sciences of the United States of America*, *95*(24), 14009–14014. https://doi.org/10.1073/pnas.95.24.14009

Danabasoglu, G., Lamarque, J. F., Bacmeister, J., Bailey, D. A., DuVivier, A. K., Edwards, J., et al. (2020). The Community Earth System Model Version 2 (CESM2). *Journal of Advances in Modeling Earth Systems*, *12*(2), e2019MS001916. https://doi.org/10.1029/2019ms001916

Dannenberg, M. P., Yan, D., Barnes, M. L., Smith, W. K., Johnston, M. R., Scott, R. L., et al. (2022). Exceptional heat and atmospheric dryness amplified losses of primary production during the 2020 US Southwest hot drought. *Global Change Biology*, *28*(16), 4794–4806. https://doi.org/10.1111/gcb.16214

Esmaeilzade, M., Kamkar, B., Galeshi, S., Ghaderifar, F., & Da Silva, J. A. T. (2015). Leaf expansion and transpiration responses of millet species to soil water deficit. *Pedosphere*, *25*(6), 834–843. https://doi.org/10.1016/s1002-0160(15)30064-3

Flatau, P. J., Walko, R. L., & Cotton, W. R. (1992). Polynomial fits to saturation vapor pressure. *Journal of Applied Meteorology and Climatology*, *31*(12), 1507–1513. https://doi.org/10.1175/1520-0450(1992)031<1507:PFTSVP>2.0.CO;2

Fu, Z., Ciais, P., Feldman, A. F., Gentine, P., Makowski, D., Prentice, I. C., et al. (2022a). Critical soil moisture thresholds of plant water stress in terrestrial ecosystems. *Science Advances*, *8*(44), eabq7827. https://doi.org/10.1126/sciadv.abq7827

Fu, Z., Ciais, P., Prentice, I. C., Gentine, P., Makowski, D., Bastos, A., et al. (2022b). Atmospheric dryness reduces photosynthesis along a large range of soil water deficits. *Nature Communications*, *13*(1), 989. https://doi.org/10.1038/s41467-022-28652-7

Gentine, P., Green, J. K., Guerin, M., Humphrey, V., Seneviratne, S. I., Zhang, Y., & Zhou, S. (2019). Coupling between the terrestrial carbon and water cycles-a review. *Environmental Research Letters*, *14*(8), 083003. https://doi.org/10.1088/1748-9326/ab22d6

Green, J. K., Seneviratne, S. I., Berg, A. M., Findell, K. L., Hagemann, S., Lawrence, D. M., & Gentine, P. (2019). Large influence of soil moisture on long-term terrestrial carbon uptake. *Nature*, *565*(7740), 476–479. https://doi.org/10.1038/s41586-018-0848-x

Grossiord, C., Buckley, T. N., Cernusak, L. A., Novick, K. A., Poulter, B., Siegwolf, R. T. W., et al. (2020). Plant responses to rising vapor pressure deficit. *New Phytologist*, *226*(6), 1550–1566. https://doi.org/10.1111/nph.16485

Guan, K. Y., Pan, M., Li, H. B., Wolf, A., Wu, J., Medvigy, D., et al. (2015). Photosynthetic seasonality of global tropical forests constrained by hydroclimate. *Nature Geoscience*, *8*(4), 284–289. https://doi.org/10.1038/Ngeo2382

Guo, R. P., Lin, Z. H., Mo, X. G., & Yang, C. L. (2010). Responses of crop yield and water use efficiency to climate change in the North China Plain. *Agricultural Water Management*, *97*(8), 1185–1194. https://doi.org/10.1016/j.agwat.2009.07.006

Gupta, A., Rico-Medina, A., & Cano-Delgado, A. I. (2020). The physiology of plant responses to drought. *Science*, *368*(6488), 266–269. https://doi.org/10.1126/science.aaz7614

Hurk, B., Kim, H. J., Krinner, G., Seneviratne, S. I., Derksen, C., Oki, T., et al. (2016). LS3MIP (v1.0) contribution to CMIP6: The Land Surface, Snow and Soil moisture Model Intercomparison Project - Aims, setup and expected outcome. *Geoscientific Model Development*, *9*(8), 2809–2832. https://doi.org/10.5194/gmd-9-2809-2016

Jung, M., Koirala, S., Weber, U., Ichii, K., Gans, F., Camps-Valls, G., et al. (2019). The FLUXCOM ensemble of global land-atmosphere energy fluxes [Dataset]. Scientific Data, *6*(1), 14. https://doi.org/10.1038/s41597-019-0076-8

Jung, M., Schwalm, C., Migliavacca, M., Walther, S., Camps-Valls, G., Koirala, S., et al. (2020). Scaling carbon fluxes from eddy covariance sites to globe: Synthesis and evaluation of the FLUXCOM approach. *Biogeosciences*, *17*(5), 1343–1365. https://doi.org/10.5194/bg-17-1343-2020

Kennedy, D., Swenson, S., Oleson, K. W., Lawrence, D. M., Fisher, R., da Costa, A. C. L., & Gentine, P. (2019). Implementing plant hydraulics in the Community Land Model, Version 5. *Journal of Advances in Modeling Earth Systems*, *11*(2), 485–513. https://doi.org/10.1029/2018ms001500

Lawrence, D. M., Fisher, R. A., Koven, C. D., Oleson, K. W., Swenson, S. C., Bonan, G., et al. (2019). The Community Land Model Version 5: Description of new features, benchmarking, and impact of forcing uncertainty. *Journal of Advances in Modeling Earth Systems*, *11*(12), 4245–4287. https://doi.org/10.1029/2018ms001583

Lawrence, P. J., & Chase, T. N. (2007). Representing a new MODIS consistent land surface in the Community Land Model (CLM 3.0). *Journal of Geophysical Research*, *112*(G1), G01023. https://doi.org/10.1029/2006jg000168

Li, X., Piao, S., Huntingford, C., Penuelas, J., Yang, H., Xu, H., et al. (2023). Global variations in critical drought thresholds that impact vegetation. *National Science Review*, *10*(5), nwad049. https://doi.org/10.1093/nsr/nwad049

Liu, L. B., Gudmundsson, L., Hauser, M., Qin, D. H., Li, S. C., & Seneviratne, S. I. (2020). Soil moisture dominates dryness stress on ecosystem production globally. *Nature Communications*, *11*(1), 4892. https://doi.org/10.1038/s41467-020-18631-1

Lyons, D. S., Dobrowski, S. Z., Holden, Z. A., Maneta, M. P., & Sala, A. (2021). Soil moisture variation drives canopy water content dynamics across the western US. *Remote Sensing of Environment*, *253*, 112233. https://doi.org/10.1016/j.rse.2020.112233

Meir, P., Wood, T. E., Galbraith, D. R., Brando, P. M., Da Costa, A. C. L., Rowland, L., & Ferreira, L. V. (2015). Threshold responses to soil moisture deficit by trees and soil in tropical rain forests: Insights from field experiments. *BioScience*, *65*(9), 882–892. https://doi.org/10.1093/biosci/biv107

Meng, L., Chambers, J., Koven, C., Pastorello, G., Gimenez, B., Jardine, K., et al. (2022). Soil moisture thresholds explain a shift from light-limited to water-limited sap velocity in the Central Amazon during the 2015-16 El Nino drought. *Environmental Research Letters*, *17*(6), 064023. https://doi.org/10.1088/1748-9326/ac6f6d

Munoz, J. (2019). ERA5-Land monthly averaged data from 1950 to present [Dataset]. Copernicus Climate Change Service (C3S) Climate Data Store (CDS). https://doi.org/10.24381/cds.68d2bb30

Munoz, J., Dutra, E., Agusti-Panareda, A., Albergel, C., Arduini, G., Balsamo, G., et al. (2021). ERA5-Land: A state-of-the-art global reanalysis dataset for land applications. *Earth System Science Data*, *13*(9), 4349–4383. https://doi.org/10.5194/essd-13-4349-2021

NCAR. (2018a). CESM2 input data [Dataset]. Retrieved from https://svn-ccsm-inputdata.cgd.ucar.edu/trunk/inputdata/lnd/clm2/rawdata/

NCAR. (2018b). Community Earth System Model Version 2 [Software]. National Center for Atmospheric Research. Retrieved from https://www.cesm.ucar.edu/models/cesm2/

Oglesby, R. J., Marshall, S., Erickson, D. J., Roads, J. O., & Robertson, F. R. (2002). Thresholds in atmosphere-soil moisture interactions: Results from climate model studies. *Journal of Geophysical Research*, *107*(D14), ACL-15. https://doi.org/10.1029/2001jd001045

Oleson, K., Lawrence, D., Bonan, G., Drewniak, B., Huang, M., Koven, C., et al. (2013). *Technical description of version 4.5 of the Community Land Model (CLM)*. National Center for Atmospheric Research (NCAR).

Park, J. (2017). Tolerance intervals from ridge regression in the presence of multicollinearity and high dimension. *Statistics & Probability Letters*, *121*, 128–135. https://doi.org/10.1016/j.spl.2016.10.016

Pastorello, G., Trotta, C., Canfora, E., Chu, H. S., Christianson, D., Cheah, Y. W., et al. (2020). The FLUXNET2015 dataset and the ONEFlux processing pipeline for eddy covariance data [Dataset]. Scientific Data, *7*(1), 225. https://doi.org/10.1038/s41597-020-0534-3

Piao, S. L., Zhang, X. P., Chen, A. P., Liu, Q., Lian, X., Wang, X. H., et al. (2019). The impacts of climate extremes on the terrestrial carbon cycle: A review. *Science China Earth Sciences*, *62*(10), 1551–1563. https://doi.org/10.1007/s11430-018-9363-5

Rogers, A., Medlyn, B. E., Dukes, J. S., Bonan, G., von Caemmerer, S., Dietze, M. C., et al. (2017). A roadmap for improving the representation of photosynthesis in Earth system models. *New Phytologist*, *213*(1), 22–42. https://doi.org/10.1111/nph.14283

Sadras, V. O., & Milroy, S. P. (1996). Soil-water thresholds for the responses of leaf expansion and gas exchange: A review. *Field Crops Research*, *47*(2–3), 253–266. https://doi.org/10.1016/0378-4290(96)00014-7

Santos, T., Keppel-Aleks, G., De Roo, R., & Steiner, A. L. (2021). Can land surface models capture the observed soil moisture control of water and carbon fluxes in temperate-to-boreal forests? *Journal of Geophysical Research: Biogeosciences*, *126*(4), e2020JG005999. https://doi.org/10.1029/2020jg005999

Shao, S. H. (2009). Application of BP neural network model in sports aerobics performance evaluation. In *2009 Pacific-Asia conference on knowledge engineering and software engineering, Proceedings* (pp. 33–35). https://doi.org/10.1109/Kese.2009.17

Soltani, A., Khooie, F. R., Ghassemi-Golezani, K., & Moghaddam, M. (2000). Thresholds for chickpea leaf expansion and transpiration response to soil water deficit. *Field Crops Research*, *68*(3), 205–210. https://doi.org/10.1016/s0378-4290(00)00122-2

Sulman, B. N., Roman, D. T., Yi, K., Wang, L. X., Phillips, R. P., & Novick, K. A. (2016). High atmospheric demand for water can limit forest carbon uptake and transpiration as severely as dry soil. *Geophysical Research Letters*, *43*(18), 9686–9695. https://doi.org/10.1002/2016gl069416

Tian, J. W., Liu, Y., Zheng, W. F., & Yin, L. R. (2022). Smog prediction based on the deep belief - BP neural network model (DBN-BP). *Urban Climate*, *41*, 101078. https://doi.org/10.1016/j.uclim.2021.101078

Toms, J. D., & Villard, M. A. (2015). Threshold detection: Matching statistical methodology to ecological questions and conservation planning objectives. *Avian Conservation and Ecology*, *10*(1), art2. https://doi.org/10.5751/ace-00715-100102

Trugman, A. T., Medvigy, D., Mankin, J. S., & Anderegg, W. R. L. (2018). Soil moisture stress as a major driver of carbon cycle uncertainty. *Geophysical Research Letters*, *45*(13), 6495–6503. https://doi.org/10.1029/2018gl078131

Vogel, M. M., Orth, R., Cheruy, F., Hagemann, S., Lorenz, R., van den Hurk, B. J. J. M., & Seneviratne, S. I. (2017). Regional amplification of projected changes in extreme temperatures strongly controlled by soil moisture-temperature feedbacks. *Geophysical Research Letters*, *44*(3), 1511–1519. https://doi.org/10.1002/2016gl071235

Wang, L., Zeng, Y., & Chen, T. (2015). Back propagation neural network with adaptive differential evolution algorithm for time series forecasting. *Expert Systems With Applications*, *42*(2), 855–863. https://doi.org/10.1016/j.eswa.2014.08.018

Wu, Y. Y., & Wu, Z. F. (2023). NPP variability associated with natural and anthropogenic factors in the tropic of cancer transect, China. *Remote Sensing (Basel)*, *15*(4), 1091. https://doi.org/10.3390/rs15041091

Xu, B. C., Deng, X. P., Zhang, S. Q., & Shan, L. (2010). Biomass partition, leaf gas exchange and water relations of alfalfa and milkvetch seedlings in response to soil drying. *Photosynthetica*, *48*(4), 481–487. https://doi.org/10.1007/s11099-010-0064-x

Xu, L., Chen, N. C., & Zhang, X. (2019). Global drought trends under 1.5 and 2 degrees C warming. *International Journal of Climatology*, *39*(4), 2375–2385. https://doi.org/10.1002/joc.5958

Yan, W. M., Zhong, Y. Q. W., & Shangguan, Z. P. (2017). Responses of different physiological parameter thresholds to soil water availability in four plant species during prolonged drought. *Agricultural and Forest Meteorology*, *247*, 311–319. https://doi.org/10.1016/j.agrformet.2017.08.017

Yang, C., Wu, J., Li, P., Wang, Y., & Yang, N. (2023). Evaluation of soil-water characteristic curves for different textural soils using fractal analysis. *Water*, *15*(4), 772. https://doi.org/10.3390/w15040772

Yang, X., Lu, M., Wang, Y., Wang, Y., Liu, Z., & Chen, S. (2021). Response mechanism of plants to drought stress. *Horticulturae*, *7*(3), 50. https://doi.org/10.3390/horticulturae7030050

Yanheng (2024). Yanheng-IAP/MyData: MyData [Dataset]. Zenodo. https://doi.org/10.5281/zenodo.10525886

Zhang, M. A. F., & Henebry, G. M. (2020). VIIRS global land surface phenology product user guide. [Dataset]. https://doi.org/10.5067/VIIRS/VNP22Q2.001

Zhou, S., Williams, A. P., Berg, A. M., Cook, B. I., Zhang, Y., Hagemann, S., et al. (2019). Land-atmosphere feedbacks exacerbate concurrent soil drought and atmospheric aridity. *Proceedings of the National Academy of Sciences of the United States of America*, *116*(38), 18848–18853. https://doi.org/10.1073/pnas.1904955116